"Mathematical Models for the Evaporation of Sessile Droplets"

Stephen K. Wilson and Brian R. Duffy

Department of Mathematics and Statistics, University of Strathclyde,

Livingstone Tower, 26 Richmond Street, Glasgow G1 1XH, United Kingdom

Final LaTeX Version

21st April 2021

Abstract

Despite its intrinsic complexity and multidisciplinary nature, considerable insight can be gained into many aspects of the evaporation of sessile droplets by using relatively simple mathematical models. In this chapter we describe some of these models and some of the insights they bring to our understanding of this fascinating problem, focusing almost entirely on models that can be solved analytically either fully or, in some cases, up to quadrature of known functions.

1 Background

The evaporation of sessile droplets is a fundamental scientific problem that is key to numerous physical and biological processes, including a wide range of industrial applications such as agrochemical spraying of plants, cooling technologies, desalination, DNA synthesis, ink-jet printing, painting, protein crystallography, and surface patterning, and, as a result, has been the subject of an explosion of analytical, experimental, and numerical investigations in recent years [see, for example, the review articles by Routh (2013), Larson (2014), Brutin & Starov (2018), and Giorgiutti-Dauphiné & Pauchard (2018)]. However, as we shall describe in this chapter, despite its intrinsic complexity and multidisciplinary nature, considerable insight can be gained into many aspects of the problem by using relatively simple mathematical models.

2 The Diffusion-Limited Model

Probably the most widely applicable, and certainly the most widely studied, mathematical model for the evaporation of a sessile droplet into a quiescent atmosphere is the so-called "diffusion-limited model"[1], which has been used with considerable success by many authors [see, for example, Picknett & Bexon (1977), Deegan *et al.* (1997, 2000), Hu & Larson (2002, 2005), McHale *et al.* (2005), Popov (2005), Poulard *et al.* (2005), Dunn *et al.* (2009a), Kulinich & Farzaneh (2009),

[1]Presumably as a consequence of the clear account of it given in the widely cited work by Popov (2005), the diffusion-limited model is, rather confusingly, sometimes also referred to as "the Popov model".

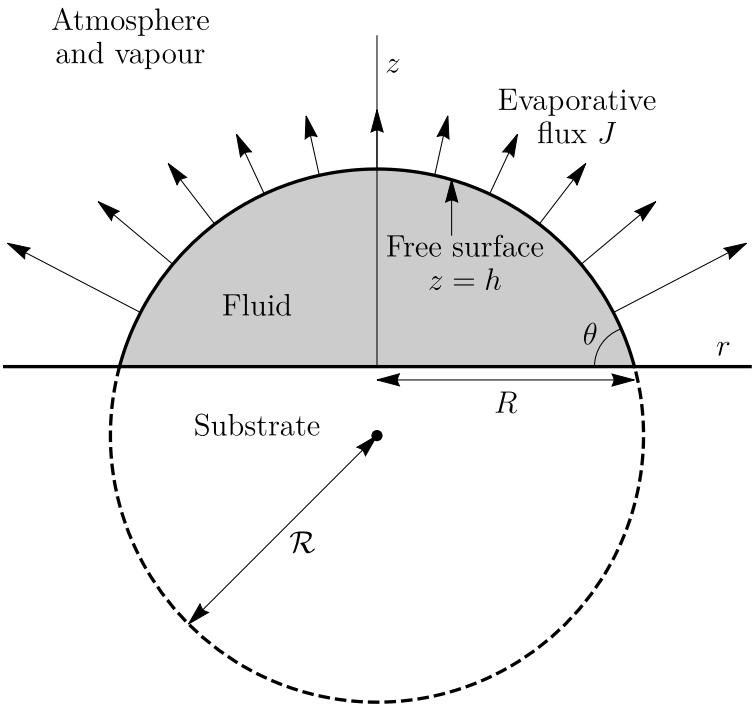

Figure 1: Geometry of the diffusion-limited evaporation of an axisymmetric droplet on a planar substrate $z = 0$. The quasi-steady free surface of the droplet, $z = h$, is a spherical cap with radius $\mathcal{R}$, contact radius R, and contact angle θ. The arrows indicate the evaporative flux from the free surface of the droplet, J, into the quiescent atmosphere.

Eggers & Pismen (2010), Gelderblom *et al.* (2012), Nguyen & Nguyen (2012), Yu *et al.* (2012), Ait Saada *et al.* (2013), Dash & Garimella (2013), Stauber *et al.* (2014, 2015a, 2015b), and Wray *et al.* (2020)]. This model is based on the assumption that the quasi-steady evaporation from the droplet is controlled by the diffusion of vapour in the quiescent atmosphere.

The geometry of the diffusion-limited evaporation of an axisymmetric droplet with free surface $z = h(r, t)$ on a planar substrate $z = 0$, where (r, ϕ, z) are the usual cylindrical polar coordinates with origin on the substrate at the centre of the droplet, and t denotes time, is shown in Figure 1. Provided that the droplet is sufficiently small (specifically, provided that it is smaller than the capillary length $\ell = (\sigma/\rho g)^{1/2}$, where σ and ρ are the surface tension and density of the fluid, and g is the magnitude of acceleration due to gravity), the quasi-steady free surface of the droplet is a spherical cap with radius $\mathcal{R} = \mathcal{R}(t)$, contact radius $R = R(t)$, and contact angle $\theta = \theta(t)$ $(0 \leq \theta \leq \pi)$ given by

$$h = -\mathcal{R}\cos\theta \pm \sqrt{\mathcal{R}^2 - r^2} \quad \text{where} \quad \mathcal{R} = \frac{R}{\sin\theta}, \tag{2.1}$$

as shown in Figure 1. Note that the physically relevant (i.e. the non-negative) part of h given by (2.1) is a single-valued function of r for $0 \leq \theta \leq \pi/2$ and for $0 \leq r \leq R$ when $\pi/2 < \theta \leq \pi$ (in which case only the "+" sign is relevant), but is a double-valued function of r for $R < r \leq \mathcal{R}$ when $\pi/2 < \theta \leq \pi$ (in which case the "+" and the "−" signs correspond to the upper and lower hemispheres, respectively). The volume of the droplet, $V = V(t)$, is given by

$$V = \frac{\pi R^3}{3}\frac{\sin\theta(2 + \cos\theta)}{(1 + \cos\theta)^2}. \tag{2.2}$$

The initial values of R, θ and V at $t = 0$ are denoted by R_0, θ_0 and V_0.

In its simplest form, the diffusion-limited model involves solving Laplace's equation $\nabla^2 c = 0$ for the concentration of vapour in the atmosphere, denoted by $c = c(r, z, t)$, subject to boundary conditions representing conditions of complete saturation at the free surface of the droplet, $c = c_{\rm sat}$ on $z = h(r, t)$, where $c_{\rm sat}$ is the constant saturation concentration of vapour, no flux of vapour through the unwetted part of the substrate, $\partial c/\partial z = 0$ on $z = 0$ for $r > R$, and the far-field condition $c \to c_\infty$ as $r^2 + z^2 \to \infty$, where c_∞ is the constant far-field concentration; note that the latter is sometimes expressed in terms of the relative humidity, denoted by H $(0 \leq H \leq 1)$, as $c_\infty = Hc_{\rm sat}$.

The solution for c was obtained by Lebedev (1965, Sections 8.10 and 8.12), who solved a mathematically equivalent electrostatics problem. In particular, this solution shows that the local evaporative mass flux from the free surface of the droplet, denoted by $J = J(r, t)$ and given by $J = -D\nabla c \cdot \mathbf{n}$ evaluated on $z = h$, where $\mathbf{n}$ is the unit outward normal to the free surface and D

is the diffusion coefficient of vapour in the atmosphere, is given by

$$J = \frac{D(c_{\rm sat} - c_\infty)}{R} \times \left[\frac{1}{2} \sin\theta + \sqrt{2}(\cosh\alpha + \cos\theta)^{3/2} \int_0^\infty \frac{\tau \cosh\theta\tau}{\cosh\pi\tau} \tanh\left[\tau(\pi-\theta)\right] P_{-1/2+i\tau}(\cosh\alpha)\, {\rm d}\tau \right], \quad (2.3)$$

where $P_{-1/2+i\tau}(\cosh\alpha)$ denotes the Legendre function of the first kind of degree $-1/2 + i\tau$ and argument

$$\cosh\alpha = \frac{r^2\cos\theta \pm R\sqrt{R^2 - r^2\sin^2\theta}}{R^2 - r^2}, \quad (2.4)$$

where the "+" and "−" signs again correspond to the upper and lower hemispheres, respectively, when $\pi/2 < \theta \leq \pi$. In particular, a local analysis in the vicinity of the contact line at $r = R$ reveals that

$$J \propto (R - r)^{-\lambda} \quad \text{as} \quad r \to R^- \quad \text{where} \quad \lambda = \frac{\pi - 2\theta}{2\pi - 2\theta}, \quad (2.5)$$

showing that J is integrably singular at the contact line when $0 \leq \theta < \pi/2$, finite and non-zero at the contact line when $\theta = \pi/2$, and zero at the contact line when $\pi/2 < \theta \leq \pi$.

At leading order in the limit of small contact angle, $\theta \to 0^+$, the free surface of the droplet is simply a parabola, namely $h = \theta(R^2 - r^2)/(2R)$, with volume $V = \pi\theta R^3/4$, and the flux is given by

$$J = \frac{2D(c_{\rm sat} - c_\infty)}{\pi\sqrt{R^2 - r^2}} \quad \text{for} \quad r < R. \quad (2.6)$$

In the special case $\theta = \pi/2$, the free surface of the droplet is a hemisphere with radius $\mathcal{R} = R$, namely $h = \sqrt{R^2 - r^2}$, with volume $V = 2\pi R^3/3$, and the flux is uniform and given by

$$J = \frac{D(c_{\rm sat} - c_\infty)}{R}. \quad (2.7)$$

In the special case $\theta = \pi$, the free surface of the droplet is a sphere of radius $\mathcal{R}$ with zero contact radius, $R = 0$, namely $h = \mathcal{R} \pm \sqrt{\mathcal{R}^2 - r^2}$, with volume $V = 4\pi\mathcal{R}^3/3$. In this case the expression for the flux (2.3) requires careful interpretation, and so, as Stauber *et al.* (2015a) pointed out, it is more convenient to use Smith & Barakat's (1975) solution for a mathematically equivalent electrostatics problem to obtain

$$J = \frac{D(c_{\rm sat} - c_\infty)}{2\mathcal{R}} \left[1 + \left(\frac{2\mathcal{R}}{h}\right)^{3/2} \int_0^\infty q \tanh q\, J_0\left(\frac{rq}{h}\right) \exp(-q)\, {\rm d}q \right], \quad (2.8)$$

where $J_0(\cdot)$ denotes the Bessel function of the first kind of order zero. In particular, the flux from the apex of the droplet (i.e. at $r = 0$ and $z = 2\mathcal{R}$) is given by

$$J = \frac{D(c_{\rm sat} - c_\infty)}{\mathcal{R}} {\rm Catalan}, \quad (2.9)$$

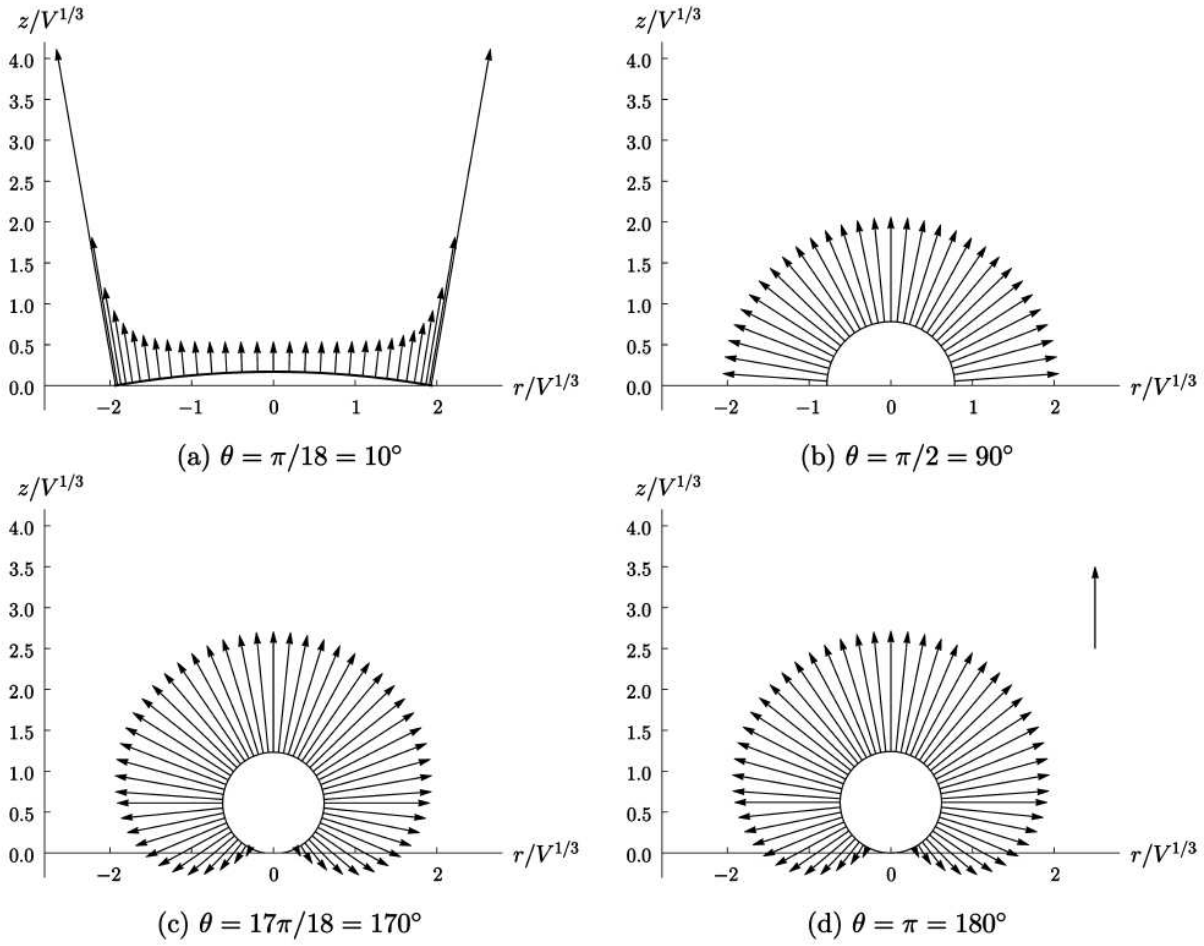

Figure 2: Scaled plots of four droplets given by (2.1) each with the same volume, V, but different contact angles, namely (a) $\theta = \pi/18 = 10°$, (b) $\theta = \pi/2 = 90°$, (c) $\theta = 17\pi/18 = 170°$, and (d) $\theta = \pi = 180°$, and different scaled contact radii, $R/V^{1/3}$, together with the corresponding scaled evaporative flux from the free surface, $JV^{1/3}/(D(c_{\rm sat} - c_\infty))$, given by (2.3) or, in the special case $\theta = \pi$, by (2.8), shown by the arrows. Note that the length of the arrows is proportional to the magnitude of $JV^{1/3}/(D(c_{\rm sat} - c_\infty))$, with the length of the reference arrow in part (d) corresponding to $JV^{1/3}/(D(c_{\rm sat} - c_\infty)) = 1$. Reprinted with permission from Stauber *et al.* (2015a, Figure 1).

where Catalan $\simeq 0.9160$ is Catalan's constant.

Figure 2, reprinted from Stauber *et al.* (2015a), shows scaled plots of four droplets given by (2.1) each with the same volume, V, but different contact angles, namely $\theta = \pi/18 = 10^\circ$ (typical of $0 \leq \theta < \pi/2$), $\theta = \pi/2 = 90^\circ$, $\theta = 17\pi/18 = 170^\circ$ (typical of $\pi/2 < \theta < \pi$), and $\theta = \pi = 180^\circ$, and different scaled contact radii, $R/V^{1/3}$, together with the corresponding scaled evaporative flux from the free surface, $JV^{1/3}/(D(c_{\rm sat} - c_\infty))$, given by (2.3) or, in the special case $\theta = \pi$, by (2.8), shown by the arrows. In particular, Figure 2 clearly illustrates the qualitatively different behaviour of the flux J in the cases $0 \leq \theta < \pi/2$, $\theta = \pi/2$ and $\pi/2 < \theta \leq \pi$. Specifically, when $0 \leq \theta < \pi/2$, J is largest (theoretically infinite) at the contact line and smallest at the apex of the droplet (i.e. at $r = 0$), when $\theta = \pi/2$ the flux is uniform and given by (2.7), and when $\pi/2 < \theta \leq \pi$ the flux is largest at the apex of the droplet and zero at the contact line.

3 The Evolution of the Droplet

Integrating the local evaporative flux J given by (2.3) over the free surface of the droplet, S, gives the total evaporative flux from the droplet, and hence, by global conservation of mass, the rate of change of the volume of the droplet, $\mathrm{d}V/\mathrm{d}t$, i.e.

$$\frac{\mathrm{d}V}{\mathrm{d}t} = -\frac{1}{\rho}\int_S J\,\mathrm{d}S = -\frac{\pi D(c_{\rm sat} - c_\infty)}{\rho}\frac{R\,g(\theta)}{(1+\cos\theta)^2}, \tag{3.1}$$

where the function $g = g(\theta)$ is defined by

$$g(\theta) = (1+\cos\theta)^2\left\{\tan\frac{\theta}{2} + 8\int_0^\infty \frac{\cosh^2\theta\tau}{\sinh 2\pi\tau}\tanh\left[\tau(\pi-\theta)\right]\,\mathrm{d}\tau\right\}. \tag{3.2}$$

For future reference, it is useful to note that $g(0) = 16/\pi$, $g(\pi/2) = 2$, and $g \sim (\pi-\theta)^3\log 2 \to 0^+$ as $\theta \to \pi^-$. Hence, recalling that V is given in terms of R and θ by (2.2), the evolution of the droplet as it evaporates satisfies the first-order nonlinear ordinary differential equation

$$\frac{\mathrm{d}}{\mathrm{d}t}\left(\frac{R^3\sin\theta(2+\cos\theta)}{(1+\cos\theta)^2}\right) = -\frac{3D(c_{\rm sat} - c_\infty)}{\rho}\frac{R\,g(\theta)}{(1+\cos\theta)^2}. \tag{3.3}$$

In particular, solving (3.3) from the initial time $t = 0$ at which $R = R_0$, $\theta = \theta_0$ and $V = V_0$ until the final time at which R and/or θ and hence V become zero determines the evolution and lifetime of the droplet. Of course, the single equation (3.3) is not on its own sufficient to determine how both R and θ evolve, and so in order to do this it is also necessary to specify what *mode* the droplet is evaporating in.[2]

[2]Of course, in reality, the mode of evaporation is determined by the details of the dominant physics near the contact line, but resolving these details inevitably introduces considerable additional complications, and so is beyond the scope of the relatively simple mathematical models described in this chapter.

4 Modes of Evaporation

The two simplest and most widely studied modes are the so-called "extreme modes", namely the constant contact radius (CR) mode and the constant contact angle (CA) mode. In the CR mode (typically observed on rough surfaces) the contact line is pinned at its initial position, i.e. $R \equiv R_0$, and the contact angle decreases to zero as the droplet evaporates, whereas in the CA mode (typically observed on smooth surfaces) the contact angle is equal to its initial value, i.e. $\theta \equiv \theta_0$, and the contact radius decreases to zero as the droplet evaporates [see, for example, Picknett & Bexon (1977)].

While these extreme modes do occur, in practice, droplets often evolve in a so-called "mixed mode" consisting of a combination of these behaviours. Various mixed modes of varying degrees of complexity have been observed, but two commonly occurring mixed modes with a "stick–slip" behaviour that naturally lend themselves to theoretical analysis are the stick–slide (SS) mode and the stick–jump (SJ) mode.

In the SS mode the droplet is initially in a CR phase with a pinned contact line, $R \equiv R_0$, but when the contact angle reaches a critical (receding) value, denoted by $\theta = \theta^*$, the contact line de-pins, and thereafter the droplet is in a CA phase with a constant contact angle, $\theta \equiv \theta^*$, until it has completely evaporated. The time at which the contact line de-pins is denoted by $t = t^*$. Note that the SS mode incorporates the two extreme modes as special cases. Specifically, when $\theta^* = 0$ the contact line never de-pins and the SS mode reduces to the CR mode, while when $\theta^* \geq \theta_0$ the contact line immediately de-pins and the SS mode reduces to the CA mode. [See, for example, Nguyen & Nguyen (2012), Dash & Garimella (2013), and Stauber *et al.* (2014, 2015b).]

In the SJ mode the droplet is again initially in a CR phrase with a pinned contact line, but when the contact angle reaches a critical (minimum) value, denoted by $\theta = \theta_{\min}$, the contact line de-pins and jumps instantaneously inwards to a new position with a smaller contact radius while the contact angle jumps instantaneously up to a critical (maximum) value, denoted by $\theta = \theta_{\max}$ ($\geq \theta_{\min}$). The pattern then repeats itself, with a (theoretically infinite) sequence of CR phases separated by instantaneous jump phases. The values of R, θ and V in the nth CR phrase ($n = 1, 2, 3, \ldots$), which lasts from $t = t_{n-1}$ to $t = t_n$, where $t = t_n$ is the time at which the nth jump phase occurs, are denoted by R_n, $\theta_n = \theta_n(t)$ and $V_n = V_n(t)$, respectively, with $R_1 = R_0$ and $\theta_1 = \theta_0$, where $\theta_{\min} \leq \theta_0 \leq \theta_{\max}$. [See, for example, Askounis *et al.* (2011), Orejon *et al.* (2011), Deitrich *et al.* (2015), and Stauber (2015).]

5 Evolution and Lifetime of a Thin Droplet

The special case of a thin droplet with small contact angle $\theta \ll 1$ is particularly amenable to further theoretical analysis, and so it is insightful to describe the evolution and lifetime of a droplet in this case before discussing them in the general case in Section 6.

At leading order in the limit of small contact angle, $\theta \to 0^+$, h and V take the simple forms given earlier, namely

$$h = \frac{\theta(R^2 - r^2)}{2R} \quad \text{and} \quad V = \frac{\pi\theta R^3}{4}, \tag{5.1}$$

and the problem for the concentration of vapour in the atmosphere becomes simply that of solving Laplace's equation $\nabla^2 c = 0$ in $z > 0$ subject to $c = c_{\rm sat}$ on $z = 0$ for $r < R$ with the other boundary condition and the far-field condition unchanged, and has a relatively simple exact solution which can be expressed in several equivalent forms, including

$$c = c_\infty + \frac{2(c_{\rm sat} - c_\infty)}{\pi} \int_0^\infty \frac{J_0(\xi r)\sin(\xi R)\exp(-\xi z)}{\xi}\,\mathrm{d}\xi \tag{5.2}$$

and

$$c = c_\infty + \frac{2(c_{\rm sat} - c_\infty)}{\pi} \sin^{-1}\frac{2R}{[(r-R)^2 + z^2]^{1/2} + [(r+R)^2 + z^2]^{1/2}}. \tag{5.3}$$

Both (5.2) and (5.3) yield the familiar expression for the local evaporative flux $J = -D\partial c/\partial z$ evaluated on $z = 0$ for $r < R$ given in (2.6). Hence the total evaporative flux from the free surface of the droplet is

$$2\pi \int_0^R J\, r\,\mathrm{d}r = 4RD(c_{\rm sat} - c_\infty), \tag{5.4}$$

and so (3.1) becomes

$$\frac{\mathrm{d}(\theta R^3)}{\mathrm{d}t} = -\frac{16RD(c_{\rm sat} - c_\infty)}{\pi\rho}. \tag{5.5}$$

[See, for example, Hu & Larson (2002) and Dunn *et al.* (2008).]

Setting $R \equiv R_0$ in (5.5) and solving for θ shows that a thin droplet evaporating in the CR mode evolves according to

$$R \equiv R_0, \quad \theta = \theta_0 - \frac{16D(c_{\rm sat} - c_\infty)}{\pi\rho R_0^2}t, \tag{5.6}$$

and so has lifetime

$$t_{\rm CR} = \frac{\pi\rho\theta_0 R_0^2}{16D(c_{\rm sat} - c_\infty)}. \tag{5.7}$$

On the other hand, setting $\theta \equiv \theta_0$ in (5.5) and solving for R shows that the same droplet evaporating in the CA mode evolves according to

$$R = R_0\left[1 - \frac{32D(c_{\rm sat} - c_\infty)}{3\pi\rho\theta_0 R_0^2}t\right]^{1/2}, \quad \theta \equiv \theta_0, \tag{5.8}$$

and so has lifetime

$$t_{\mathrm{CA}} = \frac{3\pi\rho\theta_0 R_0^2}{32D(c_{\mathrm{sat}} - c_\infty)}. \tag{5.9}$$

In particular, note that $t_{\mathrm{CA}} = 3t_{\mathrm{CR}}/2$, i.e. the lifetime of a thin droplet evaporating in the CA mode is 50% longer than that of the same droplet evaporating in the CR mode. Since the square of the radius (and hence the square of the diameter) is linear in t, equation (5.8) is sometimes referred to in the literature as "the d^2 law".

A thin droplet evaporating in the SS mode evolves according to (5.6) in the CR phase for $0 \le t \le t^*$, where

$$t^* = \frac{\pi\rho(\theta_0 - \theta^*)R_0^2}{16D(c_{\mathrm{sat}} - c_\infty)}, \tag{5.10}$$

and according to

$$R = R_0\left[1 - \frac{32D(c_{\mathrm{sat}} - c_\infty)}{3\pi\rho\theta^* R_0^2}(t - t^*)\right]^{1/2}, \quad \theta \equiv \theta^* \tag{5.11}$$

in the CA phase for $t^* \le t \le t_{\mathrm{SS}}$, and so has lifetime

$$t_{\mathrm{SS}} = \frac{\pi\rho(2\theta_0 + \theta^*)R_0^2}{32D(c_{\mathrm{sat}} - c_\infty)}. \tag{5.12}$$

In particular, note that $t_{\mathrm{SS}} = (2\theta_0 + \theta^*)t_{\mathrm{CR}}/(2\theta_0)$ which satisfies $t_{\mathrm{CR}} \le t_{\mathrm{SS}} \le t_{\mathrm{CA}}$, i.e. the lifetime of a thin droplet evaporating in the SS mode always lies between those of the same droplet evaporating in the CR and CA modes. [See Stauber *et al.* (2014, 2015b).]

A thin droplet evaporating in the SJ mode evolves according to

$$R \equiv R_n, \quad \theta = \theta_{\max} - \frac{16D(c_{\mathrm{sat}} - c_\infty)}{\pi\rho R_n^2}(t - t_{n-1}) \tag{5.13}$$

in the nth CR phrase for $t_{n-1} < t < t_n$ ($n = 1, 2, 3, \ldots$), and R jumps instantaneously down from R_n to $R_{n+1}\,(< R_n)$ and θ jumps instantaneously up from $\theta_{\min}$ to $\theta_{\max}$ in the nth jump phase at $t = t_n$. The volume of the droplet is conserved during the jump phases, i.e. $V_n = V_{n+1}$, so that

$$R_{n+1} = \left(\frac{\theta_{\min}}{\theta_{\max}}\right)^{1/3} R_n, \tag{5.14}$$

and hence

$$R_{n+1} = \left(\frac{\theta_{\min}}{\theta_{\max}}\right)^{n/3} R_0 \tag{5.15}$$

and

$$t_n = \frac{\pi\rho(\theta_{\max} - \theta_{\min})R_0^2}{16D(c_{\mathrm{sat}} - c_\infty)} \frac{\left[1 - \left(\frac{\theta_{\min}}{\theta_{\max}}\right)^{2n/3}\right]}{\left[1 - \left(\frac{\theta_{\min}}{\theta_{\max}}\right)^{2/3}\right]}. \tag{5.16}$$

Taking the limit $n \to \infty$ in (5.16) yields the lifetime of the droplet, namely

$$t_{\mathrm{SJ}} = \frac{\pi\rho(\theta_{\max} - \theta_{\min})R_0^2}{16D(c_{\mathrm{sat}} - c_\infty)} \frac{\theta_{\max}^{2/3}}{\theta_{\max}^{2/3} - \theta_{\min}^{2/3}}. \tag{5.17}$$

[See Stauber (2015).]

Note that, for all of the modes discussed above, the lifetime of the thin droplet is of the order of

$$\frac{\rho\theta_0 R_0^2}{D(c_{\text{sat}} - c_\infty)}. \tag{5.18}$$

6 Evolution and Lifetime of a General Droplet

Having discussed the behaviour of a thin droplet with small contact angle $\theta \ll 1$ in Section 5, we now describe the evolution and lifetime of a *general* droplet with *any* contact angle in the interval $0 \leq \theta \leq \pi$. The discussion in the section closely follows that of Stauber *et al.* (2014, 2015b).

Setting $R \equiv R_0$ in (3.3) yields

$$\frac{\mathrm{d}\theta}{\mathrm{d}t} = -\frac{D(c_{\text{sat}} - c_\infty)}{\rho R_0^2} g(\theta), \tag{6.1}$$

and hence a general droplet evaporating in the CR mode evolves according to the implicit expression

$$R \equiv R_0, \quad t = \frac{\rho R_0^2}{D(c_{\text{sat}} - c_\infty)} \int_\theta^{\theta_0} \frac{\mathrm{d}\tilde{\theta}}{g(\tilde{\theta})}, \tag{6.2}$$

and so has lifetime

$$t_{\text{CR}} = \frac{\rho R_0^2}{D(c_{\text{sat}} - c_\infty)} \int_0^{\theta_0} \frac{\mathrm{d}\theta}{g(\theta)}. \tag{6.3}$$

On the other hand, setting $\theta \equiv \theta_0$ in (3.3) yields

$$\frac{\mathrm{d}(R^2)}{\mathrm{d}t} = -\frac{2D(c_{\text{sat}} - c_\infty)}{\rho} \frac{g(\theta_0)}{\sin\theta_0(2 + \cos\theta_0)}, \tag{6.4}$$

and hence the same droplet evaporating in the CA mode evolves according to the explicit expression

$$R = R_0 \left[1 - \frac{2D(c_{\text{sat}} - c_\infty)}{\rho R_0^2} \frac{g(\theta_0)}{\sin\theta_0(2 + \cos\theta_0)} t\right]^{1/2}, \quad \theta \equiv \theta_0, \tag{6.5}$$

and so has lifetime

$$t_{\text{CA}} = \frac{\rho R_0^2}{2D(c_{\text{sat}} - c_\infty)} \frac{\sin\theta_0(2 + \cos\theta_0)}{g(\theta_0)}. \tag{6.6}$$

In particular, the volume of the droplet evolves according to

$$V = \frac{\pi}{3} \frac{\sin\theta_0(2 + \cos\theta_0)}{(1 + \cos\theta_0)^2} \left[R_0^2 - \frac{2D(c_{\text{sat}} - c_\infty)}{\rho} \frac{g(\theta_0)}{\sin\theta_0(2 + \cos\theta_0)} t\right]^{3/2}. \tag{6.7}$$

A general droplet evaporating in the SS mode evolves according to (6.2) in the CR phase for $0 \leq t \leq t^*$, where

$$t^* = \frac{\rho R_0^2}{D(c_{\text{sat}} - c_\infty)} \int_{\theta^*}^{\theta_0} \frac{\mathrm{d}\theta}{g(\theta)}, \tag{6.8}$$

and according to

$$R = R_0 \left[1 - \frac{2D(c_{\text{sat}} - c_\infty)}{\rho R_0^2} \frac{g(\theta^*)}{\sin\theta^*(2 + \cos\theta^*)} (t - t^*)\right]^{1/2}, \quad \theta \equiv \theta^*, \tag{6.9}$$

in the CA phase for $t^* \leq t \leq t_{\rm SS}$, and so has lifetime

$$t_{\rm SS} = \frac{\rho R_0^2}{2D(c_{\rm sat} - c_\infty)} \left[\int_{\theta^*}^{\theta_0} \frac{2\,{\rm d}\theta}{g(\theta)} + \frac{\sin\theta^*(2+\cos\theta^*)}{g(\theta^*)} \right]. \tag{6.10}$$

Note that, as expected, taking the limit $\theta \to 0^+$ and recalling that $g(0) = 16/\pi$, the expressions given above reduce to the corresponding expressions for a thin droplet given in Section 5. The behaviour in the limit $\theta_0 \to \pi^-$, corresponding to spherical and initially nearly spherical droplets, is discussed in Section 7.

For clarity of presentation in what follows, it is convenient to scale time with the timescale introduced by Stauber *et al.* (2014, 2015b), namely

$$\mathcal{T} = \frac{\rho}{2D(c_{\rm sat} - c_\infty)} \left(\frac{3V_0}{2\pi} \right)^{2/3} = \frac{\rho R_0^2}{2D(c_{\rm sat} - c_\infty)} \left(\frac{\sin\theta_0(2+\cos\theta_0)}{2(1+\cos\theta_0)^2} \right)^{2/3}, \tag{6.11}$$

and hereafter all times will be scaled with $\mathcal{T}$ unless explicitly stated otherwise.

Figures 3 and 4, reprinted from Stauber *et al.* (2014), show the lifetimes of droplets evaporating in the CR, CA and SS modes, $t_{\rm CR}$, $t_{\rm CA}$ and $t_{\rm SS}$, given by (6.3), (6.6) and (6.10), respectively, plotted as functions of the initial contact angle θ_0 for a range of values of θ^*. Note that $t_{\rm SS} = t_{\rm CA}$ for $0 < \theta_0 \leq \theta^*$. Figures 3 and 4 reveal a number of interesting and somewhat unexpected features of the dependence of the lifetimes of the droplets on θ_0 and θ^*.

In particular, Figures 3 and 4 illustrate the sometimes overlooked result first obtained, but not explicitly commented on, by Picknett & Bexon (1977) in their Figure 6, that, while it is true that for most values of θ_0 (specifically for $0 < \theta_0 < \theta_{\rm crit}$, where $\theta_{\rm crit} \simeq 2.5830 \simeq 148^\circ$) the lifetime of a droplet evaporating in the CR mode is less than that of the same droplet evaporating in the CA mode (i.e. $t_{\rm CR} < t_{\rm CA}$), for droplets with sufficiently large values of θ_0 (specifically for $\theta_{\rm crit} < \theta_0 < \pi$) the opposite is true (i.e. $t_{\rm CR} > t_{\rm CA}$). The lifetimes of identical droplets evaporating in the CR and the CA modes coincide at $\theta_0 = \theta_{\rm crit}$ (for which $t_{\rm CR} = t_{\rm CA} \simeq 0.9354$) and at $\theta_0 = \pi$ (for which $t_{\rm CR} = t_{\rm CA} = (4^{1/3}\log 2)^{-1} \simeq 0.9088$). The longest possible lifetime of a droplet evaporating in the CR mode occurs at $\theta_0 = \theta_{\rm crit}$, while the longest possible lifetime of a droplet evaporating in the CA mode is $t_{\rm CA} = 1$ and occurs at $\theta_0 = \pi/2$.

Since the SS mode is a simple combination of the extreme modes, it would be natural to assume that the lifetime of a droplet evaporating in this mode would always lie between those of the same droplet evaporating in the extreme modes (i.e. that either $t_{\rm CR} < t_{\rm SS} < t_{\rm CA}$ or $t_{\rm CA} < t_{\rm SS} < t_{\rm CR}$) for all values of θ_0 in the range $\theta^* < \theta_0 < \pi$. However, as Figures 3 and 4 show, while this is always true for $0 < \theta_0 < \pi/2$, it is not, in general, true for $\pi/2 < \theta_0 < \pi$. Specifically, if we denote the unique value of θ_0 in the range $\pi/2 \leq \theta_0 \leq \theta_{\rm crit}$ at which $t_{\rm SS} = t_{\rm CA}$ (shown with the dots in Figure 3(b)) by $\hat{\theta}_0 = \hat{\theta}_0(\theta^*)$, then $t_{\rm SS} > \max(t_{\rm CR}, t_{\rm CA})$ for $\hat{\theta}_0 < \theta_0 < \pi$ when $0 < \theta^* < \pi/2$ (as shown

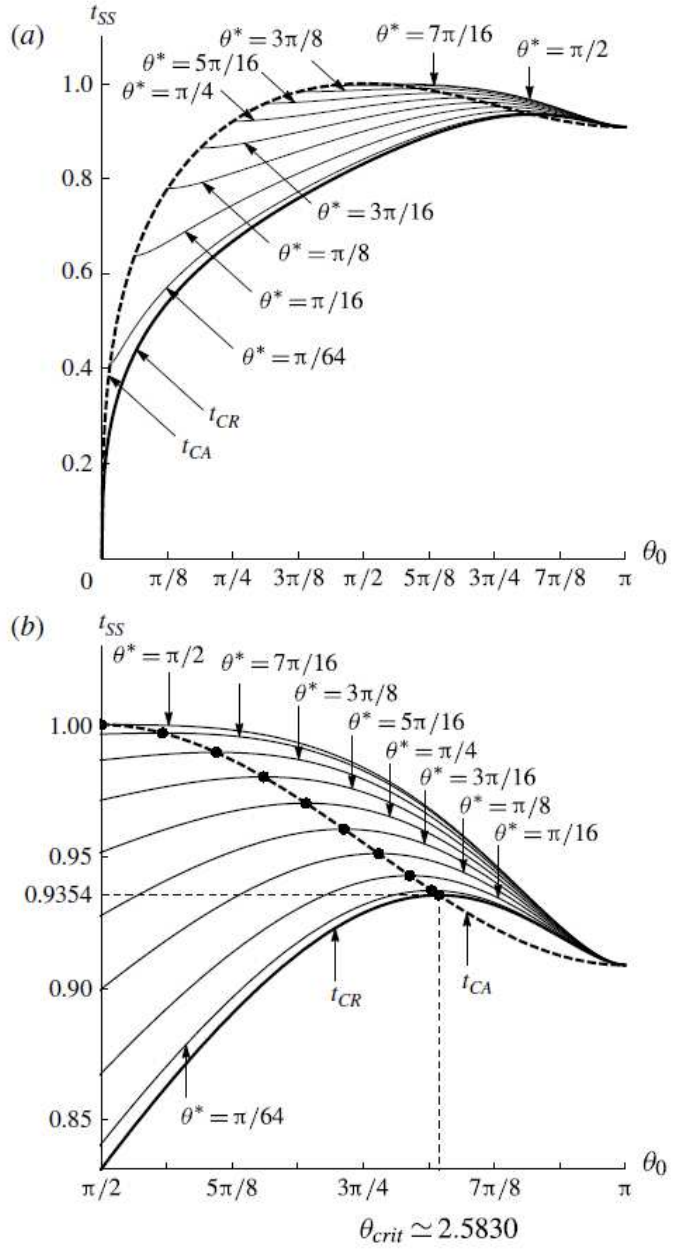

Figure 3: Lifetimes of droplets evaporating in the CR, CA and SS modes, $t_{\rm CR}$ (thick solid curve), $t_{\rm CA}$ (thick dashed curve) and $t_{\rm SS}$ (thin solid curves) plotted as functions of the initial contact angle θ_0 for a range of values of θ^* in the interval $0 < \theta^* \leq \pi/2$. Part (b) shows the behaviour in the range $\pi/2 \leq \theta_0 \leq \pi$ in greater detail, and the dots correspond to the unique value of $\theta_0 = \hat{\theta}_0(\theta^*)$ in the range $\pi/2 \leq \theta_0 \leq \pi$ at which $t_{\rm SS} = t_{\rm CA}$. Reprinted with permission from Stauber *et al.* (2014, Figure 3).

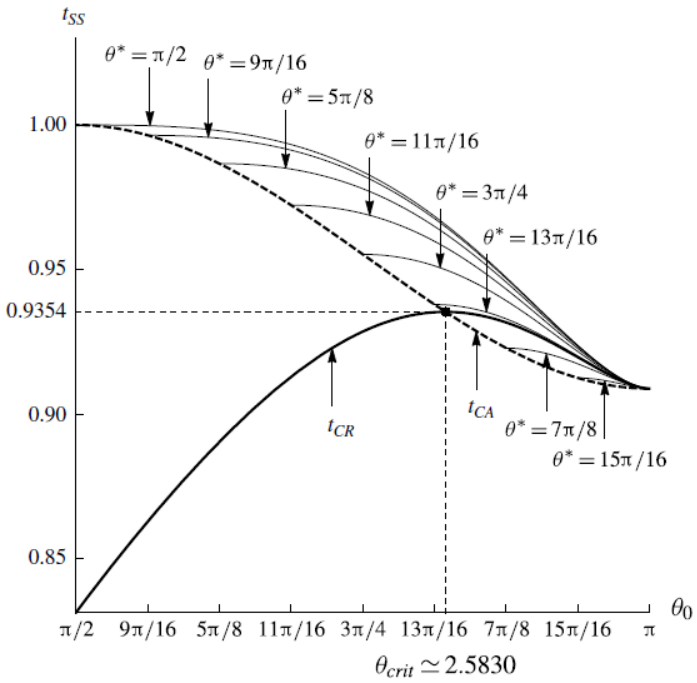

Figure 4: As Figure 3(a), except for a range of values of θ^* in the interval $\pi/2 \leq \theta^* < \pi$. Reprinted with permission from Stauber *et al.* (2014, Figure 4).

in Figure 3(b)) and for $\theta^* < \theta_0 < \pi$ when $\pi/2 < \theta^* < \pi$ (as shown in Figure 4). The longest possible lifetime of a droplet evaporating in the SS mode occurs at $\theta_0 = \hat{\theta}_0$ when $0 \leq \theta^* \leq \pi/2$ and at $\theta_0 = \pi/2$ when $\pi/2 \leq \theta^* \leq \pi$. In particular, Figure 3 and 4 show that the longest possible lifetime of a droplet evaporating in either the CR, the CA or the SS mode for any values of θ_0 and θ^* is $t_{\rm CA}(\pi/2) = 1$, corresponding to a hemispherical droplet evaporating in the CA mode. Note that the results of Stauber *et al.* (2014) presented in Figure 3 and 4 treat θ_0 and θ^* as independent parameters. Subsequently Stauber *et al.* (2015b) examined the consequences of a physically credible relationship between them based on the unbalanced Young force.

Figure 5, reprinted from Stauber *et al.* (2015a), shows illustrative examples of the evolutions of (a) the contact angle θ, (b) the scaled contact radius $R/V_0^{1/3}$, and (c) the scaled volume V/V_0 plotted as functions of scaled time $t/\mathcal{T}$ for droplets with four different initial contact angles, namely $\theta_0 = \pi/18 = 10^\circ$, $\theta_0 = \pi/2 = 90^\circ$, $\theta_0 = \theta_{\rm crit} \simeq 2.5830 \simeq 148^\circ$, and $\theta_0 = 17\pi/18 = 170^\circ$, in the CR and CA modes given by (6.2) and (6.5), respectively. In particular, Figure 5 shows that while (as previously mentioned) the lifetimes of droplets evaporating in the CR and CA modes coincide when $\theta_0 = \theta_{\rm crit}$, the evolutions of θ, R and V for the two modes are very different.

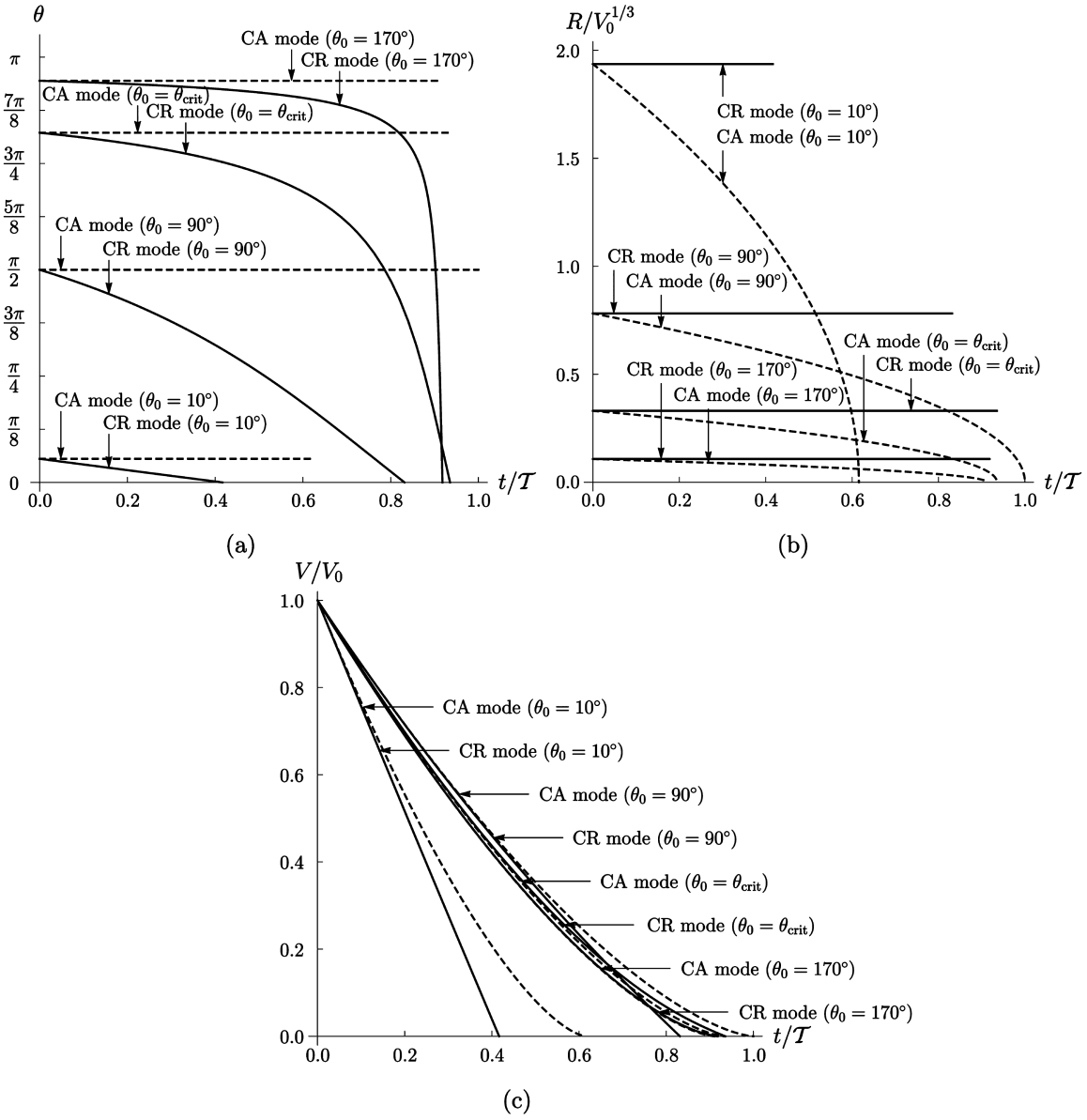

Figure 5: Evolutions of (a) the contact angle θ, (b) the scaled contact radius $R/V_0^{1/3}$, and (c) the scaled volume V/V_0 plotted as functions of scaled time $t/\mathcal{T}$ for droplets with four different initial contact angles $\theta_0 = \pi/18 = 10°$, $\theta_0 = \pi/2 = 90°$, $\theta_0 = \theta_{\rm crit} \simeq 2.5830 \simeq 148°$, and $\theta_0 = 17\pi/18 = 170°$, in the CR and CA modes shown with solid and dashed lines, respectively. Reprinted with permission from Stauber *et al.* (2015a, Figure 2).

7 Spherical and Initially Nearly Spherical Droplets

In the special case of a spherical droplet evaporating in either the CR or the CA mode both the contact radius $R \equiv R_0 = 0$ and the contact angle $\theta \equiv \theta_0 = \pi$ remain constant throughout the evolution of the droplet (i.e. the extreme modes coincide).

As Stauber *et al.* (2015a) described, either integrating the flux given by (2.8) over the free surface of the droplet or taking the limit $\theta \to \pi^-$ in (3.3) and recalling that $g(\theta) \sim (\pi - \theta)^3 \log 2$, shows that a spherical droplet evaporating in either of the extreme modes evolves according to

$$\frac{\mathrm{d}\mathcal{R}}{\mathrm{d}t} = -\frac{D(c_{\mathrm{sat}} - c_\infty)\log 2}{\rho \mathcal{R}}, \tag{7.1}$$

which has the exact solution

$$\mathcal{R} = \mathcal{R}_0 \left[1 - \frac{2D(c_{\mathrm{sat}} - c_\infty)\log 2}{\rho \mathcal{R}_0^2} t\right]^{1/2}, \tag{7.2}$$

where $\mathcal{R}_0 = \mathcal{R}(0)$ is the initial radius of the sphere, and so the droplet has unscaled lifetime

$$t_\pi = \frac{\rho \mathcal{R}_0^2}{2D(c_{\mathrm{sat}} - c_\infty)\log 2} = \frac{\rho}{2D(c_{\mathrm{sat}} - c_\infty)} \left(\frac{3V_0}{2\pi}\right)^{2/3} \frac{1}{4^{1/3}\log 2}, \tag{7.3}$$

and its volume evolves according to

$$V = \frac{4\pi \mathcal{R}_0^3}{3} \left[1 - \frac{2D(c_{\mathrm{sat}} - c_\infty)\log 2}{\rho \mathcal{R}_0^2} t\right]^{3/2}. \tag{7.4}$$

In particular, as previously mentioned, from (6.11) and (7.3), the (scaled) lifetime of the droplet is $t_\pi = (4^{1/3}\log 2)^{-1} \simeq 0.9088$.

Taking the limit $\theta_0 \to \pi^-$ in (6.1) reveals that the contact angle of an initially nearly spherical droplet evaporating in the CR mode evolves according to

$$\theta = \pi - \left(1 - \frac{t}{t_\pi}\right)^{-1/2} (\pi - \theta_0) + O(\pi - \theta_0)^3 \tag{7.5}$$

as $\theta_0 \to \pi^-$, which remains close to $\theta = \pi$ until t is near to t_π (i.e. the droplet remains nearly spherical until close to the end of its evaporation), in agreement with the corresponding evolution in the case $\theta_0 = 17\pi/18 = 170^\circ$ shown in Figure 5(a). Similarly, taking the limit $\theta_0 \to \pi^-$ in (6.4) reveals that the contact radius of an initially nearly spherical droplet evaporating in the CA mode evolves according to

$$R = \left(\frac{3V_0}{4\pi}\right)^{1/3} \left(1 - \frac{t}{t_\pi}\right)^{1/2} (\pi - \theta_0) + O(\pi - \theta_0)^3 \tag{7.6}$$

as $\theta_0 \to \pi^-$, which remains close to $R = 0$ for all t (i.e. the droplet remains nearly spherical throughout its entire evaporation), in agreement with the corresponding evolution in the case

$\theta_0 = 17\pi/18 = 170^\circ$ shown in Figure 5(b). For both of the extreme modes, the volume of the droplet evolves according to

$$V = V_0 \left(1 - \frac{t}{t_\pi}\right)^{3/2} + O(\pi - \theta_0)^2 \tag{7.7}$$

as $\theta_0 \to \pi^-$. In other words, as Stauber *et al.* (2015a) pointed out, the extreme modes become indistinguishable on strongly hydrophobic substrates (i.e. on substrates with $\theta_0 \simeq \pi$).

8 Evaporative Cooling

Evaporation of vapour from the free surface of the droplet requires latent heat and so causes spatially non-uniform evaporative cooling of the droplet and its surroundings.

In the simplest version of the diffusion-limited model described in Section 2, the evaporative problem for the concentration of vapour in the atmosphere is decoupled from the thermal problem for the temperatures of the droplet, the substrate and the atmosphere, denoted by $T = T(r, z, t)$, $T^{\rm s} = T^{\rm s}(r, z, t)$ and $T^{\rm a} = T^{\rm a}(r, z, t)$, respectively. Hence, once the local evaporative flux has been determined, the evaporative cooling of the droplet and its surroundings can be determined by solving the appropriate equations for T, $T^{\rm s}$ and $T^{\rm a}$ subject to the local energy balance

$$\mathcal{L}J = (k^{\rm a}\nabla T^{\rm a} - k\nabla T)\cdot\mathbf{n} \quad \text{on} \quad z = h, \tag{8.1}$$

where $\mathcal{L}$ is the latent heat of vaporisation, k, $k^{\rm s}$ and $k^{\rm a}$ are the thermal conductivities of the droplet, the substrate and the atmosphere, and $\mathbf{n}$ is again the unit outward normal to the free surface of the droplet, together with conditions representing continuity of temperature and heat flux at the boundaries between the three regions. This is, in general, difficult to do without resorting to numerical methods, but analytical progress can be made in the special case of a thin droplet on a thin substrate.

For a thin droplet with small contact angle $\theta \ll 1$ on a thin substrate of thickness $h^{\rm s} \ll R_0$, then, provided that $k^{\rm a} \ll k/\theta_0$ and $k^{\rm a} \ll R_0 k^{\rm s}/h^{\rm s}$ (i.e. provided that, as is likely to be the case in practice, the atmosphere is a relatively poor conductor), the problem for $T^{\rm a}$ decouples from that for T and $T^{\rm s}$. Assuming the transport of heat in the droplet and the atmosphere is due solely to thermal conduction, T and $T^{\rm s}$ satisfy $\partial^2 T/\partial z^2 = 0$ in $0 < z < h$ and $\partial^2 T^{\rm s}/\partial z^2 = 0$ in $-h^{\rm s} < z < 0$ for $r < R$ subject to $\mathcal{L}J = -k\partial T/\partial z$ on $z = h$, $T = T^{\rm s}$ and $-k\partial T/\partial z = -k^{\rm s}\partial T^{\rm s}/\partial z$ on $z = 0$, and $T^{\rm s} = T_0$ on $z = -h^{\rm s}$ for $r < R$, where T_0 is the prescribed constant temperature on the lower

surface of the substrate, with solution

$$T = T_0 - \frac{2D\mathcal{L}(c_{\rm sat} - c_\infty)}{\pi\sqrt{R^2 - r^2}}\left(\frac{z}{k} + \frac{h^{\rm s}}{k^{\rm s}}\right) \quad \text{for} \quad 0 < z < h, \tag{8.2}$$

$$T^{\rm s} = T_0 - \frac{2D\mathcal{L}(c_{\rm sat} - c_\infty)}{\pi k^{\rm s}\sqrt{R^2 - r^2}}(z + h^{\rm s}) \quad \text{for} \quad -h^{\rm s} < z < 0, \tag{8.3}$$

for $r < R$. In particular, the solutions (8.2) and (8.3) quantify the evaporative cooling of the droplet and the substrate, respectively. [See, for example, Dunn *et al.* (2008).]

A more sophisticated version of the diffusion-limited model in which the saturation concentration $c_{\rm sat}$ is taken to be a known function of temperature T, i.e. $c_{\rm sat} = c_{\rm sat}(T)$, which couples the evaporative and thermal problems, was formulated and analysed by Dunn *et al.* (2008, 2009a) and Sefiane *et al.* (2009) (the latter of whom also included the dependence of the diffusion coefficient D on the pressure of the atmosphere). In particular, these authors showed that the thermal properties of the substrate can have a significant effect on the rate of evaporation. Subsequently Ait Saada *et al.* (2013) and Schofield *et al.* (2021) developed this approach to calculate the effects of the thermal properties of the system on the lifetime of a droplet evaporating in the extreme modes. In particular, Figure 6, reprinted from Schofield *et al.* (2021), shows the lifetimes of droplets of water evaporating in the CR and the CA modes on aluminium, HDPE and PTFE substrates plotted as functions of the scaled initial contact angle θ_0/π, and illustrates that the thermal conductivity of the substrate can have a strong influence on the lifetime of the droplet, especially for droplets with large initial contact angles. For comparison, Figure 6 also shows the corresponding lifetimes according to the simplest (decoupled) version of the diffusion-limited model previously shown in Figures 3 and 4.

The extreme situation of a substrate with high thermal resistance and/or when the saturation concentration depends strongly on temperature was analysed by Dunn *et al.* (2009b) and Schofield *et al.* (2018). In particular, these authors showed that for a thin droplet on a thin substrate the lifetime of the droplet is of the order of

$$\frac{\rho\theta_0 R_0 \mathcal{L} h^{\rm s} c'_{\rm sat}(T_\infty)}{k^{\rm s}(c_{\rm sat}(T_\infty) - c_\infty)}, \tag{8.4}$$

where $c'_{\rm sat}(T) = {\rm d}c_{\rm sat}/{\rm d}T$ is the derivative of $c_{\rm sat}$ with respect to T, which can be much longer than the usual timescale given in equation (5.18), confirming that the lifetime of an evaporating droplet can be significantly extended by strong thermal effects.

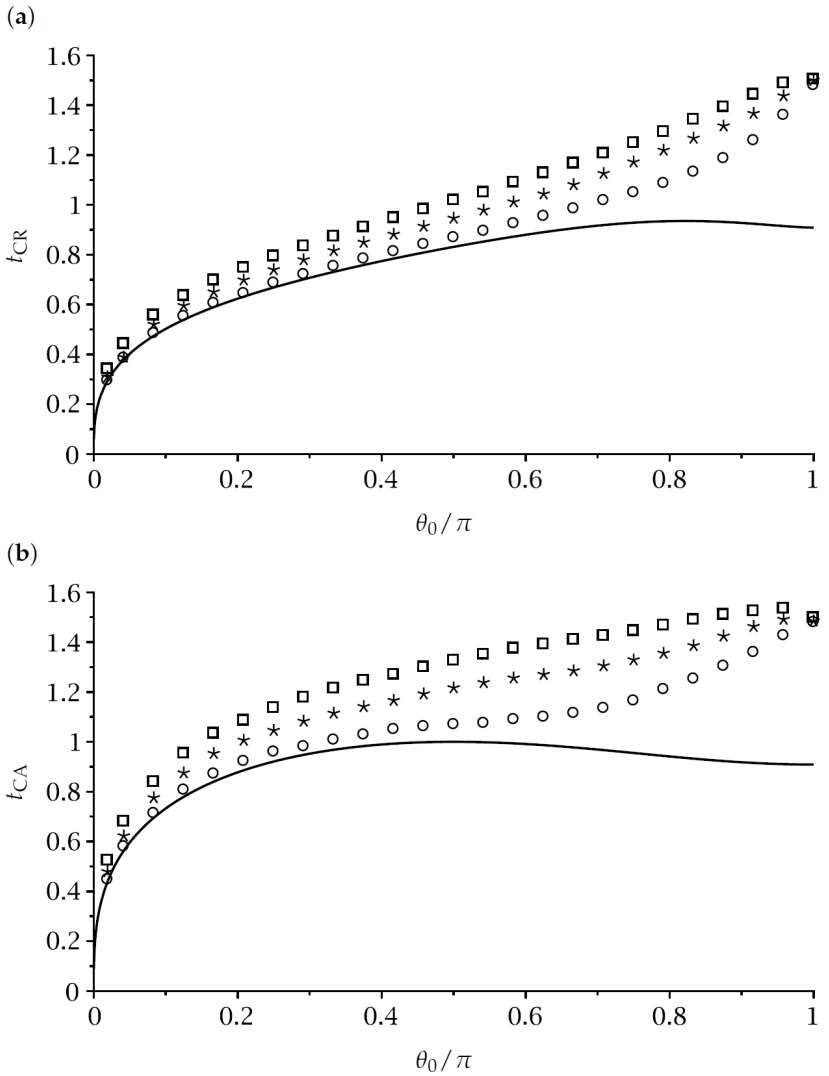

Figure 6: Lifetimes of droplets of water with initial contact radius $R_0 = 1$ mm evaporating in (a) the CR mode, t_{CR}, and (b) the CA mode, t_{CA}, into air with $T_\infty = 295$ K on aluminium ($k^{\mathrm{s}} = 237$ W m^{-1} K^{-1}, circles), HDPE ($k^{\mathrm{s}} = 0.50$ W m^{-1} K^{-1}, stars) and PTFE ($k^{\mathrm{s}} = 0.25$ W m^{-1} K^{-1}, squares) substrates of thickness $h^{\mathrm{s}} = 1$ mm plotted as functions of the scaled initial contact angle θ_0/π. The solid lines show the corresponding lifetimes according to the simplest (decoupled) version of the diffusion-limited model previously shown in Figures 3 and 4. Reprinted with permission from Schofield *et al.* (2021, Figure 6).

9 Extensions and Generalisations

Although not discussed here, the theoretical predictions of the models described in this chapter (and similar models based on the same physical assumptions) have been found to be in remarkably good agreement with the results of physical experiments in a wide range of situations. However, like any mathematical model, the relatively simple models described in this chapter have their limitations and shortcomings and there are many ways in which they can be extended, developed and improved. Here we briefly mention just three such extensions amongst many others.

Firstly, inspired by the pioneering work of Deegan *et al.* (1997, 2000) in recent years there has been considerable interest in the manner in which solid particles initially suspended within a droplet are deposited onto the substrate as it evaporates and, in particular, in the characteristic "coffee-stain" or "ring-stain" which typically forms near to the location of the contact line of a pinned droplet [see, for example, the review articles by Larson (2014) and Mampallil & Eral (2018)]. Several authors have developed mathematical models for the advection of the particles towards the contact line as a droplet evaporates, including Boulogne *et al.* (2017), who obtained analytical predictions for the accumulation of particles at the contact line of a thin droplet with the spatially non-uniform evaporative flux (2.6) and a spatially uniform evaporative flux (the latter being an appropriate model for the evaporation of a droplet on a wet hydrogel rather than a dry substrate).

Secondly, as described in Section 8, even the simplest version of the diffusion-limited model shows that the evaporation causes spatially non-uniform evaporative cooling, and if the surface tension of the droplet depends on temperature, the resulting spatially non-uniform temperature distribution within the droplet can lead to a thermocapillary-driven flow within it. Many authors have used a range of mathematical models of varying degrees of sophistication to analyse aspects of this phenomenon, including Hu & Larson (2005) and Ristenpart *et al.* (2007).

Thirdly, while the vast majority of theoretical and experimental work on droplet evaporation has, like the present chapter, focused on single droplets, in practice, most droplets do not occur in isolation, and so the interactions between multiple evaporating droplets are of considerable scientific and practical interest. An interesting recent theoretical development is the work by Wray *et al.* (2020), who developed an asymptotic model for the evaporation of an arbitrary arrangement of thin droplets. This model captures the "shielding" effect that each droplet has on the evaporation of its neighbours, and was used by the authors to obtain explicit expressions for the evolution and the lifetimes of a pair of identical droplets evaporating in the CR, CA and SS modes which generalise those given in Section 6 for an isolated droplet and quantify how the effect of shielding lengthens the lifetime of the droplets. For example, the lifetime of a pair of identical droplets with contact

radius R_0 whose centres are a distance $B\,(>2R_0)$ apart evaporating in the CR mode is

$$t_{\mathrm{CR}} = \frac{\pi\rho\theta_0 R_0^2}{16D(c_{\mathrm{sat}}-c_\infty)}\left(1+\frac{2}{\pi}\arcsin\frac{R_0}{B}\right), \tag{9.1}$$

which shows that the effect of shielding is to increase the lifetime of the droplets by as much as 33% (achieved in the limit when the droplets are touching, i.e. in the limit $B \to 2R_0^+$) relative to that of an isolated droplet given by (5.7) (achieved in the limit when the droplets are far apart, i.e. in the limit $B \to \infty$). Wray *et al.* (2020) also obtained qualitatively similar results for pairs of identical droplets evaporating in the CA and the SS modes. A rather different theoretical approach was taken by Schofield *et al.* (2020), who used a conformal-mapping technique to obtain closed-form solutions for the evolution and lifetime of a pair of identical two-dimensional "droplets" which also quantify how the effect of shielding lengthens the lifetime of these droplets.

Acknowledgements

The authors wish to thank Hannah-May D'Ambrosio (University of Strathclyde) and Prof. Khellil Sefiane (University of Edinburgh) for their insightful comments on a draft version of this chapter.

References

1. A. F. Routh, Drying of thin colloidal films, *Rep. Prog. Phys.*, 2013, **76**, 046603.

2. R. G. Larson, Transport and deposition patterns in drying sessile droplets, *AIChE J.*, 2014, **60**, 1538.

3. D. Brutin and V. Starov, Recent advances in droplet wetting and evaporation, *Chem. Soc. Rev.*, 2018, **47**, 558.

4. F. Giorgiutti-Dauphiné and L. Pauchard, Drying drops, *Euro. Phys. J. E*, 2018, **41**, 32.

5. R. G. Picknett and R. Bexon, The evaporation of sessile or pendant drops in still air, *J. Coll. Int. Sci.*, 1977, **61**, 336.

6. R. D. Deegan, O. Bakajin, T. F. Dupont, G. Huber, S. R. Nagel and T. A. Witten, Capillary flow as the cause of ring stains from dried liquid drops, *Nature*, 1997, **389**, 827.

7. R. D. Deegan, O. Bakajin, T. F. Dupont, G. Huber, S. R. Nagel and T. A. Witten, Contact line deposits in an evaporating drop, *Phys. Rev. E*, 2000, **62**, 756.

8. H. Hu and R. G. Larson, Evaporation of a sessile droplet on a substrate, *J. Phys. Chem. B*, 2002, **106**, 1334.

9. H. Hu and R. G. Larson, Analysis of the effects of Marangoni stresses on the microflow in an evaporating sessile droplet, *Langmuir*, 2005, **21**, 3972.

10. G. McHale, S. Aqil, N. J. Shirtcliffe, M. I. Newton and H. Y. Erbil, Analysis of droplet evaporation on a superhydrophobic surface, *Langmuir*, 2005, **21**, 11053.

11. Y. O. Popov, Evaporative deposition patterns: spatial dimensions of the deposit, *Phys. Rev. E*, 2005, **71**, 036313.

12. C. Poulard, G. Guéna and A. M. Cazabat, Diffusion-driven evaporation of sessile drops, *Journal of Physics: Condensed Matter*, 2005, **17**, S4213.

13. G. J. Dunn, S. K. Wilson, B. R. Duffy, S. David and K. Sefiane, The strong influence of substrate conductivity on droplet evaporation, *J. Fluid Mech.*, 2009a, **623**, 329.

14. S. A. Kulinich and M. Farzaneh, Effect of contact angle hysteresis on water droplet evaporation from super-hydrophobic surfaces, *Applied Surface Science*, 2009, **255**, 4056.

15. J. Eggers and L. M. Pismen, Nonlocal description of evaporating drops, *Phys. Fluids*, 2010, **22**, 112101.

16. H. Gelderblom, O. Bloemen and J. H. Snoeijer, Stokes flow near the contact line of an evaporating drop, *J. Fluid Mech.*, 2012, **709**, 69.

17. T. A. H. Nguyen and A. V. Nguyen, On the lifetime of evaporating sessile droplets, *Langmuir*, 2012, **28**, 1924.

18. Y.-S. Yu, Z. Wang and Y.-P. Zhao, Experimental and theoretical investigations of evaporation of sessile water droplet on hydrophobic surfaces, *J. Coll. Int. Sci.*, 2012, **365**, 254.

19. M. Ait Saada, S. Chikh and L. Tadrist, Evaporation of a sessile drop with pinned or receding contact line on a substrate with different thermophysical properties, *Int. J. Heat Mass Trans.*, 2013, **58**, 197.

20. S. Dash and S. V. Garimella, Droplet evaporation dynamics on a superhydrophobic surface with negligible hysteresis, *Langmuir*, 2013, **29**, 10785.

21. J. M. Stauber, S. K. Wilson, B. R. Duffy and K. Sefiane, On the lifetimes of evaporating droplets, *J. Fluid Mech.*, 2014, **744**, R2.

22. J. M. Stauber, S. K. Wilson, B. R. Duffy and K. Sefiane, Evaporation of droplets on strongly hydrophobic substrates, *Langmuir*, 2015a, **31**, 3653.

23. J. M. Stauber, S. K. Wilson, B. R. Duffy and K. Sefiane, On the lifetimes of evaporating droplets with related initial and receding contact angles, *Phys. Fluids*, 2015b, **27**, 122101.

24. A. W. Wray, B. R. Duffy and S. K. Wilson, Competitive evaporation of multiple sessile droplets, *J. Fluid Mech.*, 2020, **884**, A45.

25. N. N. Lebedev, *Special Functions and their Applications* (Revised English edition translated and edited by R. A. Silverman), Prentice-Hall Inc., Englewood Cliffs, NJ, USA, 1965.

26. G. S. Smith and R. Barakat, Electrostatics of two conducting spheres in contact, *Appl. Sci. Res.*, 1975, **30**, 418.

27. A. Askounis, D. Orejon, V. Koutsos, K. Sefiane and M. E. R. Shanahan, Nanoparticle deposits near the contact line of pinned volatile droplets: size and shape revealed by atomic force microscopy, *Soft Matter*, 2011, **7**, 4152.

28. D. Orejon, K. Sefiane and M. E. R. Shanahan, Stick-slip of evaporating droplets: substrate hydrophobicity and nanoparticle concentration, *Langmuir*, 2011, **27**, 12834.

29. E. Dietrich, E. S. Kooij, X. Zhang, H. J. W. Zandvliet and D. Lohse, Stick-jump mode in surface droplet dissolution, *Langmuir*, 2015, **31**, 4696.

30. J. M. Stauber, On the Evaporation of Sessile Droplets, PhD Thesis, University of Strathclyde, Glasgow, 2015.

31. G. J. Dunn, S. K. Wilson, B. R. Duffy, S. David and K. Sefiane, A mathematical model for the evaporation of a thin sessile liquid droplet: comparison between experiment and theory, *Colloids and Surfaces A: Physicochemical and Engineering Aspects*, 2008, **323**, 50.

32. K. Sefiane, S. K. Wilson, S. David, G. J. Dunn and B. R. Duffy, On the effect of the atmosphere on the evaporation of sessile droplets of water, *Phys. Fluids*, 2009, **21**, 062101.

33. F. G. H. Schofield, D. Pritchard, S. K. Wilson and K. Sefiane, The lifetimes of evaporating sessile droplets of water can be strongly influenced by thermal effects, *Fluids*, 2021, **6**, 141.

34. G. J. Dunn, S. K. Wilson, B. R. Duffy and K. Sefiane, Evaporation of a thin droplet on a thin substrate with a high thermal resistance, *Phys. Fluids*, 2009b, **21**, 052101.

35. F. G. H. Schofield, S. K. Wilson, D. Pritchard and K. Sefiane, The lifetimes of evaporating sessile droplets are significantly extended by strong thermal effects, *J. Fluid Mech.*, 2018, **851**, 231.

36. D. Mampallil and H. B. Eral, A review on suppression and utilization of the coffee-ring effect, *Advances in Colloid and Interface Science*, 2018, **252**, 38.

37. F. Boulogne, F. Ingremeau and H. A. Stone, Coffee-strain growth dynamics on dry and wet surfaces, *J. Phys.: Condens. Matter*, 2017, **29**, 074001.

38. W. D. Ristenpart, P. G. Kim, C. Domingues, J. Wan and H. A. Stone, Influence of substrate conductivity on circulation reversal in evaporating drops, *Phys. Rev. Lett.*, 2007, **99**, 234502.

39. F. G. H. Schofield, A. W. Wray, D. Pritchard and S. K. Wilson, The shielding effect extends the lifetimes of two-dimensional sessile droplets, *J. Eng. Math.*, 2020, **120**, 89.